Nanoscience and Nanotechnology Letters
Vol. 3, 41–48, 2011

Closed π-Electron Network in Large Polyhedral Multi-Shell Carbon Nanoparticles

A. I. Shames[1,*], I. Felner[2], V. Yu. Osipov[3], E. A. Katz[4,5], E. Mogilko[6], J. Grinblat[7], A. M. Panich[1], V. P. Belousov[8], I. M. Belousova[8], and A. N. Ponomarev[9]

[1] *Department of Physics, Ben-Gurion University of the Negev, Be'er-Sheva 84105, Israel*
[2] *Rakah Institute of Physics, Hebrew University of Jerusalem, Givat Ram 84105, Israel*
[3] *Ioffe Physical-Technical Institute, Polytechnicheskaya 26, St.Petersburg, 194021, Russia*
[4] *Department of Solar Energy and Environmental Physics, J. Blaustein Institutes for Desert Research, Ben-Gurion University of the Negev, Sede Boqer 84990, Israel*
[5] *Ilze-Katz Institute for Nanoscale Science and Technology, Ben-Gurion, University of the Negev, Be'er-Sheva 84105, Israel*
[6] *Department of Physics and Center for Superconductivity, Bar-Ilan University, Ramat Gan 52900, Israel*
[7] *Department of Chemistry, Bar-Ilan University, Ramat Gan 52900, Israel*
[8] *Institute for Laser Physics, SIC Vavilov SOI, St. Petersburg 199034, Russia*
[9] *JSC Astrin-Holding, St. Petersburg 19809, Russia*

High Resolution Transmission Electron Microscopy (HRTEM) reveals a polyhedral multi-shell fullerene-like structure of astralen carbon nanoparticles. The polyhedra consist of large flat graphitic faces connected by defective edge regions with presumably pentagon-like structure. The faces comprise a stacking of 20–50 planar graphene sheets with inter-sheet distance of ~0.340 nm. Average sizes of the particles and their flat faces are ~40 nm and ~15 nm, respectively. Astralen particles are suggested to have defect-free sp^2 flat faces and all defects condense at their polyhedral edges. Multi-frequency Electron Paramagnetic Resonance (EPR) spectra of polycrystalline astralen samples reveal two main signals: a very broad signal with $\Delta H_{pp} > 1$ T and an asymmetric relatively narrow signal that consists of two Lorentzian components in $g = 2.00$ region. The intensities of all X-band EPR signals show no changes on decreasing temperature down to $T = 4$ K. Magnetic susceptibility demonstrates strong temperature dependent orbital diamagnetism. All unusual magnetic features of astralen are attributed to prevalent itinerant spins.

Keywords: Carbon Onions, Multi-Shell Polyhedral Nanoparticles, Magnetic Resonance, Magnetic Susceptibility, Delocalized Electrons.

The discovery[1] of *buckminsterfullerene*, C_{60}, a new variety of carbon, has generated enormous interest in many areas of physics, chemistry and material science. Now, the term *fullerenes* is used for various all-carbon closed-cage molecules in which π-conjugated carbon hexagon rings are condensed to form a closed surface with the participation of pentagon rings. Recently, much attention has turned towards novel fullerene-related materials, carbon *nanocapsules* or carbon *onions* that consist of concentric fullerene-like shells. Ugarte[2] observed that carbon soot particles and tubular graphitic structure are transformed into quasi-spherical carbon onions by intense electron-beam irradiation in a transmission electron microscope. The structure of spherical onions cannot be described in terms of perfect fullerene-like shells made of pentagonal and hexagonal carbon rings only and requires introduction of a large number of defects, such as heptagonal–pentagonal pairs.[3] As a result, π-electrons in spherical onions are localized in very small domains of sp^2 graphitic sheets, and do not act as conduction electrons.[4] On the contrary, polyhedral onions have an ordered graphitic structure, presumably with defect-free sp^2 flat faces and a definite number of pentagon-like defects condense at the polyhedral cusps.[5] Accordingly, delocalized π-electrons in polyhedral onions can act as conduction electrons. This effect should be enhanced as sizes of polyhedra increase. Nowadays, knowledge on the correlation between structure and electronic properties of individual carbon onions is very limited. To the best of our knowledge, such comprehensive studies were performed only for spherical and

*Author to whom correspondence should be addressed.

small polyhedral onions produced by high temperature (HT) vacuum annealing of nanodiamond particles.[4, 6–8] For the present study we adopted large carbon particles, so-called astralens, obtained by thermal vaporization of graphite anode by arc discharge using special conditions of vaporization, extraction and subsequent treatment of cathodic deposit.[9] The polyhedral fullerene-like structure of astralen particles had been recently[10] confirmed and analyzed by High Resolution Transmission Electron Microscopy (HRTEM), X-ray Diffraction (XRD) and Raman spectroscopy studies. X-band Electron Paramagnetic Resonance (EPR) and NMR techniques[10] revealed unusual electronic and magnetic properties of astralen and demonstrated their qualitative difference from those of the carbon onions obtained from HT treated (HTT) nanodiamonds.[4, 8] The present work extends understanding of the origin of magnetism in astralen system by means of multi-frequency EPR and magnetic susceptibility measurements.

HRTEM provides direct evidence that astralen particles have a polyhedral multi-shell structure with a hollow interior (Fig. 1(a)). The average diameter of astralen particles is ~40 nm. The polyhedra consist of flat graphitic faces with average size of ~15 nm connected by defective edge regions (Fig. 1(b)). The faces comprise a stacking of 20–50 planar graphene sheets with an inter-sheet distance of ~0.340 nm. HRTEM also reveals that the astralen samples under study are quite pure and homogeneous ones: they contain predominantly the multi-shell nanoparticles but not other nanocarbon entities. Recent XRD and Raman data[10] confirm this conclusion. The amorphous graphite texture in the background of astralen particles' images in Figure 1 belong to the Cu/carbon grid.

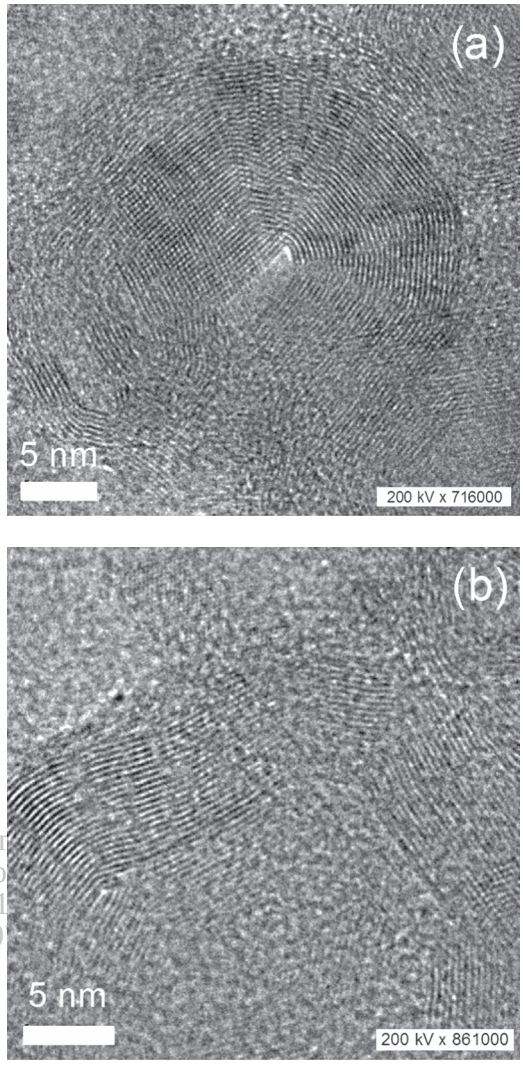

Fig. 1. Representative HRTEM images of astralen nanoparticles.

Room temperature (RT, $T = 300$ K) X-band ($\nu \sim 9.4$ GHz) EPR spectrum of astralen particles, recorded within the maximal scan width of 1 T, consists of two clearly distinguished components:[10] a very broad signal with the line width $\Delta H_{pp} > 1$ T (Fig. 2(a), black line) and an asymmetric narrow (ΔH_{pp} of the order of several mT) signal centered close to $g = 2.00$ (Fig. 2(b), olive line). The sharp low field ($g \sim 4.3$) EPR line in these spectra (see Fig. 2(a)) belongs to Fe^{3+} ions originating from the glass of the capillary tube and is used as an external intensity reference. All spectral components (both broad and narrow ones) are found to be practically independent of the ambient pressure and show no observable changes when the sample was pumped out to the vacuum level better than 2×10^{-5} mbar at both RT and $T = 600$ K. Here it is worth mentioning that careful analysis of power dependences of the $g = 2.00$ signals evidences that dioxygen somehow affects the signal (will be reported elsewhere). The solid lines in Figure 3 (upper spectra) show RT spectra of the $g = 2.00$ EPR signal at three microwave frequencies: S-band ($\nu \sim 3.5$ GHz), black solid line in Figure 3(a); X-band, magenta solid line in Figure 3(b) and Q-band ($\nu \sim 34$ GHz), green solid line in Figure 3(c). These RT spectra may be successfully simulated as superposition of two Lorentzian components[11, 12] (Figs. 3(a–c), lower spectra) of different line widths, g-factors and intensities. Integral intensities ratios and g-factors (see linear plot of resonance fields H_r in Fig. 4(a)) for both components are found to be frequency independent: ratio of doubly integrated intensities (DIN) $DIN_2/DIN_1 \sim 10–13$, $g_1 = 2.0034 \pm 0.0002$ for the narrow component and $g_2 = 2.007 \pm 0.001$ for the broad one. On the other hand the line widths are frequency dependent: $\Delta H_{pp1} = 0.63 \pm 0.05$ mT, $\Delta H_{pp2} = 2.6 \pm 0.3$ mT (S-band); $\Delta H_{pp1} = 0.67 \pm 0.05$ mT, $\Delta H_{pp2} = 3.6 \pm 0.3$ mT (X-band); and $\Delta H_{pp1} = 0.86 \pm 0.05$ mT, $\Delta H_{pp2} = 5.9 \pm 0.3$ mT (Q-band) (Fig. 4(b)). Amounts of paramagnetic centers of different types were estimated at X-band[10] and found to be $N_{s1} \sim 5 \times 10^{17}$ spins g^{-1} for the narrow Lorentzian component, $N_{s2} \sim 7 \times 10^{18}$ spins g^{-1} for the broad one. Estimating the number of localized and quasi-localized spins per each astralen

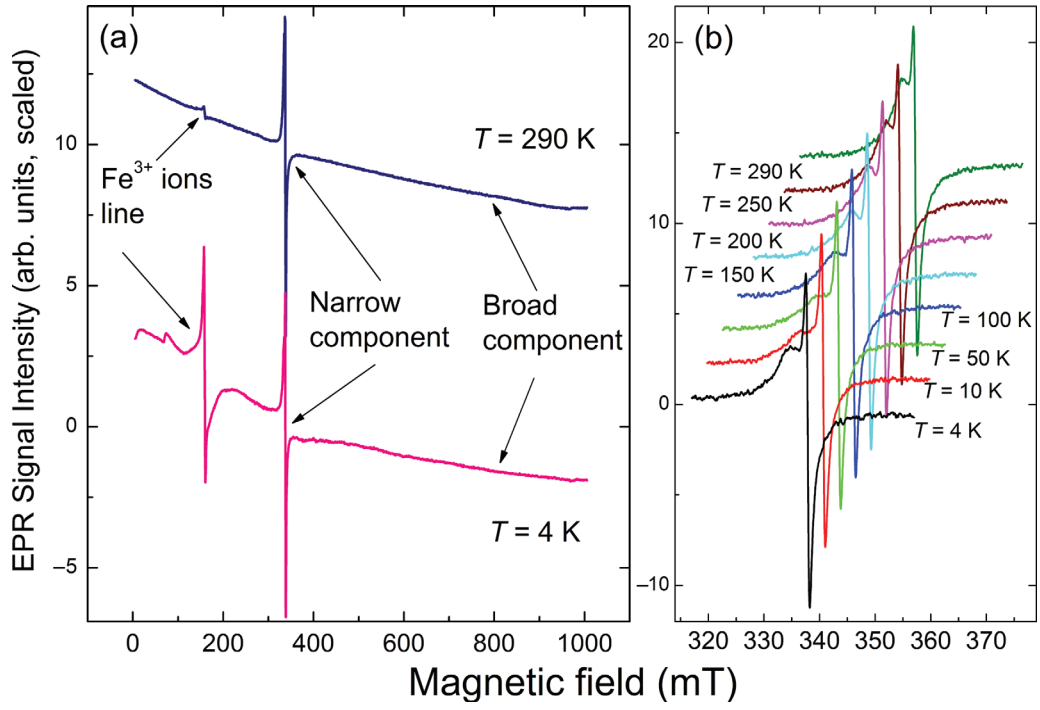

Fig. 2. EPR spectra of astralen particles: (a) general view at $T = 290$ K (navy line) and $T = 4$ K (pink line) recorded at the same instrumental conditions, $\nu = 9.465$ GHz; (b) $g = 2.00$ EPR signal recorded at different temperatures, $\nu = 9.466$ GHz. Spectra were recorded at the same instrumental conditions.

particle we found that each particle contains (totally, in all graphene layers) ca. 40 localized spins and ca. 500 quasi-localized spins.

X-band EPR measurements at variable temperatures $4\text{K} \leq T \leq 300$ K were done on the sample sealed under vacuum. EPR signals associated with astralen demonstrate unusual temperature evolution.[10] Intensities of the broad and both $g = 2.00$ components, unlike EPR signals of the most paramagnetic species, do not obey the Curie law (Fig. 2(a)). Figure 2(b) obviously demonstrates very weak changes of the astralen $g = 2.00$ EPR signals' intensity on decreasing temperature from RT down to $T =$ 4 K whereas the EPR signal of paramagnetic Fe^{3+} ions from the sample tube, being under the same conditions as the astralen sample, shows evident temperature dependence of its intensity—see corresponding low-field signals in Figure 2(a). Figure 5(a) represents temperature dependences of the intensities of two $g = 2.00$ components. These intensities were obtained by different methods: DIN by direct double numerical integration of the experimental spectra (narrow and broad Lorentzian components together), S by simple calculation using experimental data for the narrow Lorentzian component intensity and the line width as $S = I_{pp} \times (\Delta H_{pp})^2$ (where I_{pp} is peak-to-peak intensity of the narrow component) and by simulation of experimental $g = 2.00$ EPR line (narrow and broad Lorentzian components separately). Both line width and g-factor of the broad Lorentzian component slightly increase on temperature decrease and then jump-down at $T = 4$ K (Figs. 5(b, c)). The narrow component broadens for a few hundredths of mT and its g-factor insignificantly decreases from 2.0034 down to 2.0030.

Multi-frequency EPR data unambiguously justify the attribution of an asymmetric axial-like polycrystalline pattern at $g = 2.00$ to the superposition of two separate Lorentzian components that have been proposed for the description of X-band spectra.[10] Indeed, changes in spectral resolution of these lines from S-band to Q-band (Fig. 3) perfectly agree with this model. Another interesting result of the multi-frequency data is the frequency dependence of the line widths of both Lorentzian components (Fig. 4(b)). The Lorentzian shapes of the $g = 2.00$ signals observed indicate the exchange interaction between spins of the same type. At higher frequencies exchange, being independent of quantum, is less effective in averaging of differences that causes frequency dependent linear line broadening—so called g-strain effect.[13] Thus multi-frequency EPR data reveal variations of the microenvironment of each individual spin smoothed by exchange interactions. Here it is worth mentioning that strong non-resonant microwave absorption found for astralen sample does not contradict the Lorentzian line shapes observed for the $g = 2.00$ EPR lines. Assuredly just the Lorentzian, but not Dysonian line shape seems to be quite a natural one for de-aggregated conducting carbon nanoparticles with particle dimensions that are smaller than the skin depth at the highest microwave frequency used ~34 GHz (which exceeds 300 nm even for metallic copper and gold).

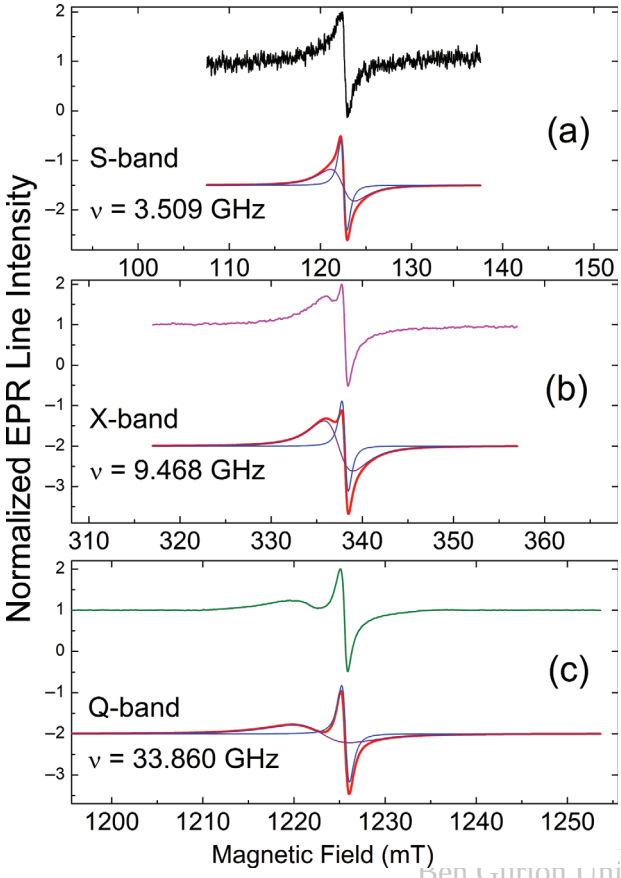

Fig. 3. RT EPR spectra of astralen particles recorded at different microwave frequencies: (a) S-band, $\nu = 3.905$ GHz (black line); (b) X-band, $\nu = 9.468$ GHz (magenta line) and (c) Q-band, $\nu = 33.860$ GHz (green line). Upper spectra in each panel—experimental data, lower spectra—deconvolution into two Lorentzian lines: best least square fit (red lines), narrow component (blue lines) and broad component (violet lines).

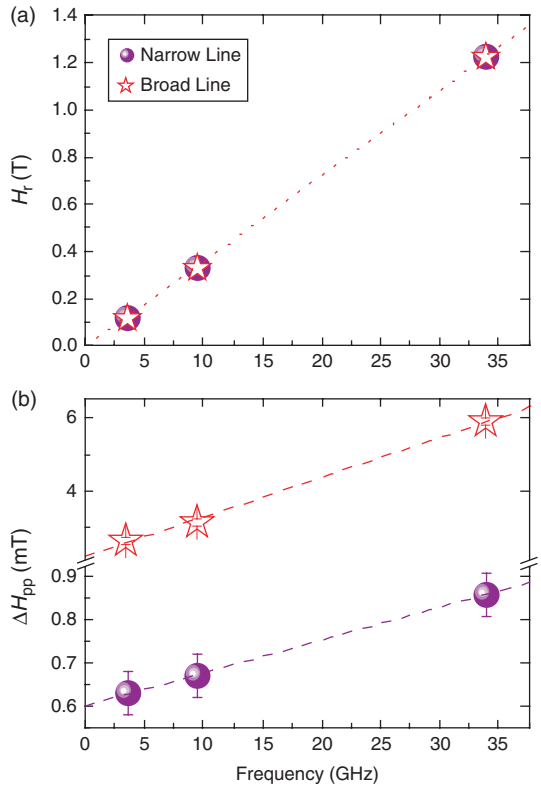

Fig. 4. Frequency dependence of resonance fields H_r (a) and line widths ΔH_{pp} (b) obtained for each Lorentzian component by simulation of RT spectra in Figure 3. Lines are best linear fits of these data.

Except for the very broad signal with $\Delta H_{pp} > 1$ T, relatively narrow $g = 2.00$ components revealed in our study have also been observed in X-band EPR spectra of various nanographites[14, 15] and HTT nanodiamonds.[4, 6–8] However, both temperature dependence of signals intensity (spectra are observed well above 100 K) and the lack of the microwave saturation for $g = 2.00$ lines[10] in conjunction with HRTEM, XRD and Raman data on samples' purity and homogeneity allow excluding direct analogies of EPR signals in astralen with the like signals in nanographites. The most adequate resemblance may be traced with EPR spectra of HTT nanodiamonds. Thus, narrow ($\Delta H_{pp} \sim 0.7$–0.9 mT) Lorentzian lines with $g = 2.0020$–2.0022, which intensities obey the Curie law, have been found in quasi-spherical carbon onions obtained by "soft" thermal treatment.[4, 8] Broad ($\Delta H_{pp} \sim 1$–10.9 mT, depending on the oxygen pressure) Lorentzian lines with $g = 2.0010$–2.0014, which intensities show features characteristic of Pauli or mixed Pauli-Curie paramagnetism, have been found in small polyhedral particles obtained by more intensive thermal treatment.[6, 8] These relatively broad EPR signals were attributed to non-bonding π-electrons localized at the marginal regions of a nanographite sheet having a zig-zag shape.[9] In general, the $g = 2.00$ EPR signals in astralen (Figs. 2, 3) look like signals of the aforementioned types and belong to some defects in carbon network. However, there are several noteworthy differences found for the signals in astralen in comparison with those observed in carbon onions produced by HTT nanodiamonds:

(a) low sensitivity of EPR signals in astralen to oxygen pressure;

(b) temperature independent paramagnetism within the very broad temperature range; and

(c) higher g-values.[10]

The electronic properties of nanographite systems including their magnetic and conducting characteristics depend on sizes of defect-free domains in graphene sheets, L_a.[8] In our astralen particles the size of these defect-free domains coincides with the size of flat graphene faces. On the other hand, the L_a is comparable (and even exceeds) the known size for nano-graphite particles exhibiting an abrupt transition (in the range of 5–15 nm) to the bulk graphite properties.[16] The most unusual feature of the EPR properties observed in astralen is the Pauli-type behavior of EPR magnetic susceptibilities for all signals in the

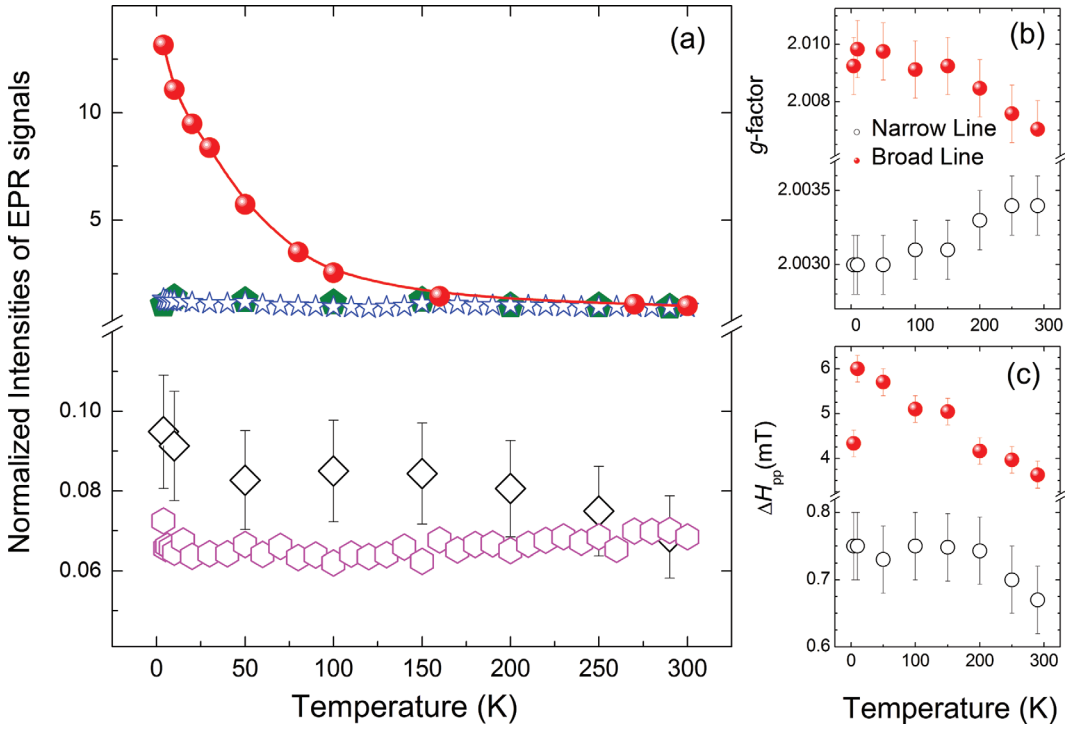

Fig. 5. (a) Temperature dependences of the integral intensities of $g = 2.00$ EPR signals': stars—experimental DIN obtained by numerical integration of both $g = 2.00$ signals; hexagons—intensity S of the narrow Lorentzian signal calculated as $S = I_{pp} \times (\Delta H_{pp})^2$; intensities of the narrow (diamonds) and broad (pentagons) Lorentzian signals obtained by simulation; circles—intensity S of paramagnetic Fe^{3+} ions signal. Signal intensities are normalized to the same values at $T = 300$ K; Temperature dependences of g-factors (b) and line widths (c) for the broad (red closed circles) and narrow (open black circles) Lorentzian $g = 2.00$ EPR signals.

wide temperature range, especially in the low-temperature region 4–50 K (Fig. 5(a)). Following Osipov et al.[8] we speculate that the narrow and broad Lorentzian EPR components observed in astralen are associated with localized and quasi-localized spins, respectively, though the corresponding defects in astralens and the onions produced by HTT of nanodiamonds can be of different origin. Indeed, in astralen both the quasi-localized and the localized spins are associated with the corner-condensed defects and interact with numerous itinerant spins which belong to the same graphene layer of the astralen particle. Accordingly, unlike the case of small multi-layered particles produced by HTT of nanodiamonds, where the treatment conditions determine the observed features of paramagnetic behavior for the edge-state spins, both localized and quasi-localized spins (the $g = 2.00$ lines) show the same temperature independent paramagnetism down to 4 K. In our opinion, the unusual properties of the EPR active spins observed in astralen samples can be understood within the framework of the well-developed theory of electron resonance of localized electron spins in metals.[17] Following this theory the main factor determining all EPR features is the ratio of magnetic susceptibilities of conduction electrons χ_s and localized paramagnetic centers χ_d: $\chi_r = \chi_d/\chi_s$. In the cases of $\chi_r \ll 1$ the conduction electrons' properties will predominate and EPR signals of localized paramagnetic centers will behave in the same manner as signals of conduction electrons spin resonance, i.e., their intensities will demonstrate the Pauli-type paramagnetism. When $\chi_r > 1$ the properties of EPR signal will be determined by properties of localized paramagnetic centers, that is the Curie-type paramagnetism. The similar, almost temperature independent, EPR signals have been observed in metallic (or semiconducting) multiwall carbon nanotubes (MWCNT) which $\chi_{EPR}(T)$ has been interpreted in terms of a dominant, slightly temperature dependent Pauli contribution and a small Curie component.[18] In principle this interpretation well coincides with the aforementioned relations that are correct for metals. Thus, the assumption on the high value of ratio between the dynamic susceptibility of itinerant charge carriers (delocalized π-electrons and/or defect driven holes) and total dynamic susceptibility of localized and quasi-localized spins in astralen system exhaustively explains the unusual temperature dependences of the EPR signals observed in astralen. Several experimental observations support this assumption. Although experimental data obtained do not allow direct estimation of charge carrier number or the Pauli susceptibility (by means of the Kotosonov approach[19]) there are several indirect evidences for the attribution of astralen to a system with strong conducting properties. First of all, the intensive non-resonant microwave absorption observed (which leads to the Q-value reduction) is a characteristic for conducting graphite samples. Another argument in

favor is detection of the very broad ($\Delta H_{pp} > 1$ T) EPR signals that have been observed in both astralen and conducting graphite samples. The origin of this line is rather the effect of non-resonant microwave absorption due to magnetic field dependent magnetoresistance observed in heavily doped Ga-As semiconductors[20] than conduction electron spin resonance line, as it was earlier supposed in our preceding article.[10] Indeed, the latter hypothesis provides extremely high number of charge carriers that is hardly compatible with the total number of carbon atoms in astralen and declared perfection of its graphene layers. It is worth mentioning that in nanodiamond-originated multishell nanoparticles, where the ratio between the narrow signal (localized spins) and the broad one (quasi-localized π-electrons) was found to be ca. 20, i.e., comparable with that found in astralen, both broad and narrow EPR signals demonstrate the Curie-type paramagnetism below 100 K.[6] This means that the quasi-localized π-electrons only, even supposing they obeys the predominant Pauli-type behavior, which was found to be correct just above 100 K,[6, 8] can not suppress the Curie-type behavior in a way observed in astralen. Our hypothesis on fulfilling the $\chi_r \ll 1$ condition in astralen assumes the availability of strong exchange interaction between itinerant carriers and localized spins, responsible for the broad and narrow $g = 2.00$ EPR signals. It was shown[15] that this exchange interaction leads to the shift of the resonance field for localized spins due to the effective hyperfine field induced by conduction electrons. This effect may explain low-field shift of resonance fields (positive g-shifts mentioned above) of both EPR lines attributed to localized and quasi-localized spins in comparison with the same values found in carbon onions produced by HTT of nanodiamonds.[4, 6–8] The latter samples demonstrate the mixed Curie-Pauli paramagnetism and evidently higher χ_r values that reduces corresponding exchange g-shifts. The temperature-dependent ^{13}C NMR spin-lattice relaxation data in astralen supplies additional arguments in favor of the aforementioned hypothesis: the slope value in the $T_1(T)$ plot for astralen $T_{1n} \sim T^{-0.612}$ falls between the metallic behavior, $T_{1n} \sim T^{-1}$ (Korringa relation), and the semiconductor behavior, $T_{1n} \sim T^{-0.5}$.[10]

Figure 6(a) represents temperature dependence of DC magnetic susceptibility $\chi(T)$ for the polycrystalline astralen sample (curve 1) in comparison with $\chi(T)$ obtained on the multishell polyhedral nanographite particles of 5–7 nm size and crystallite size of the graphene planes ~3.5 nm-NG110 sample taken from Ref. [8] (curve 2). The measurements were carried out at $H =$ 1 T. Within the entire temperature range, even at lowest temperatures, $\chi(T)$ of astralen has negative values exceeding, by modulus, 7×10^{-6} emu/g that clearly evidences pronounced diamagnetic properties of this material. At $T > 22$ K the $\chi(T)$-curve shows positive slope whereas at $T < 22$ K the slope is negative. The former is a characteristic feature for the temperature behavior of orbital diamagnetism χ_{orb} in graphite-like materials

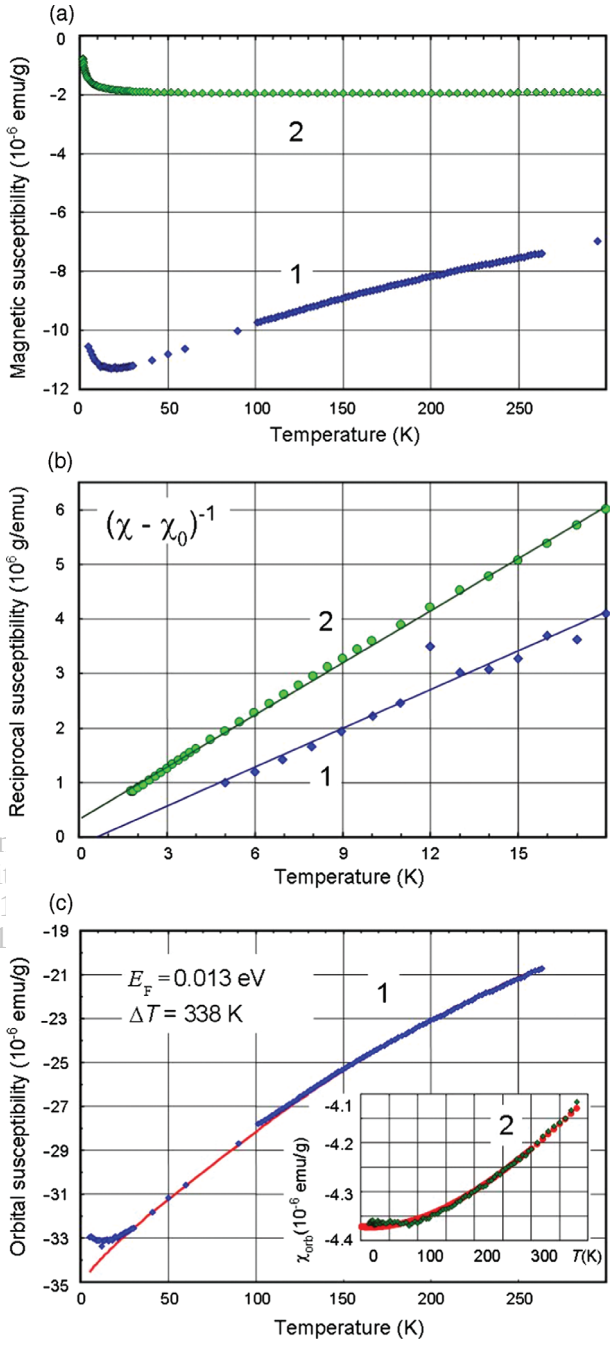

Fig. 6. Temperature dependences of DC magnetic susceptibility and its contributions for two multishell polyhedral nanographite samples: large—astralen and small–NG110. Curves marked 1 relate to polycrystalline astralen, curves marked 2–to NG110. (a) Experimental data of DC magnetic susceptibility $\chi(T)$; (b) CW-contribution to $\chi(T)$ plotted in coordinates $[\chi(T) - \chi_0]^{-1}$ versus T; (c) in-plane orbital diamagnetism $\chi_{orb} \approx 3 \times [\chi(T) - \chi_{cw} - \chi_{core}]$. Straight lines in (b) are best linear fits of experimental points obtained at $T < 18$ K by varying of χ_0 parameter. Red solid lines in (c) are best fits of experimental points using the phenomenological Kotosonov approach for χ_{orb} with E_F and ΔT as fitting parameters.

where the absolute value $|\chi_{orb}|$ declines with temperature decrease and the latter is typical for the Curie-Weiss (CW) contribution $\chi_{cw} = C/(T - \Theta)$ (where C and Θ are the Curie constant and Weiss parameter) to the static

magnetic susceptibility originating from localized magnetic moments (spins) of intrinsic paramagnetic defects or transition metal ions impurities. The observed χ value is the sum of the four terms $\chi(T) = \chi_{cw} + \chi_{core} + \chi_P + 1/3 \times \chi_{orb}$. Here χ_{core} is temperature independent diamagnetic susceptibility of isolated carbon atoms (-0.5×10^{-6} emu/g), χ_P is the Pauli susceptibility which is roughly proportional to the density of states (DOS) and χ_{orb} is in-plane orbital susceptibility of the graphite-like material in the field H normal to the graphene planes. The factor 1/3 is associated with the directional average for powdered samples. Figure 6(b) (curve 1) represents the CW-contribution that was extracted from the experimental data and plotted in coordinates $[\chi(T) - \chi_0]^{-1}$ versus T. Here χ_0 is temperature independent fitting parameter (-1.154×10^{-5} emu/g) found for getting the best linear dependence of $[\chi(T) - \chi_0]^{-1}$ within the temperature region below 20 K. The Weiss parameter was found to be $\Theta = +0.59$ K indicating the weak ferromagnetic exchange between uncoupled spins. The slope of this curve unambiguously provides us with the C value that allows independent (of EPR measurements) determination of the spin density in this graphite system that found to be $N_s = 6.77 \times 10^{18}$ spin/g. Following Ref. [8] these spins are related to $S = 1/2$ spins localized at the edges of the graphene layers i.e., with the intrinsic edge defects of the graphite matrix. It is worth mentioning that the concentration of the edge spins in astralen somewhat exceeds (or almost close to) the same parameter found[8] in NG110—see Figure 6(b) (curve 2). Supposing $1/3 \times \chi_{orb} \gg \chi_P$ (that, in fact, does not work so well for the NG110 sample) one can easily determine in-plane orbital susceptibility $\chi_{orb} \approx 3 \times [\chi(T) - \chi_{cw} - \chi_{core}]$—experimental data points are shown in Figure 6(c) and may be satisfactorily fitted by the phenomenological equation proposed in late eighties by Kotosonov for the description of χ_{orb} in nanostructured graphite materials of various origin (Fig. 1(c), red solid curve):[19]

$$\chi_{orb}[\text{emu/g}] = -1.3625 \times 10^{-3} \gamma_0 \frac{\text{sech}^2(E_F/2k_B(T + \Delta T))}{(T + \Delta T)} \quad (1)$$

Here, E_F is the Fermi energy, ΔT is an additional temperature term to account for the nonthermal electron scattering by the boundaries and structural defects of the graphite nanoparticle, $\gamma_0 \cong 3$ eV is a 2D band parameter, k_B is the Boltzmann constant. As a matter of fact, the phenomenological ΔT parameter is determined by the "smearing" of the DOS spectrum of the material due to the relaxation of π-carriers through scattering on the crystallite edges and intrinsic point-like defects. Indeed, crystallite edges (together with point-like defects inside the graphene planes) work as very effective scattering centers for conductive π-carries. Smaller in-plane crystallite sizes correspond to larger ΔT parameters.

In contrast with the approach of Ref. [8], for the fitting of the experimental points by Eq. (1) we took into account the temperature dependence of Fermi energy $E_F(T)$ that appears in Eq. (1) as the fitting parameter. For the description of $E_F(T)$ we used the model of infinite 2D graphene sheet with linear behavior of the density of electronic states within π- and $\pi*$- bands in the wide (-0.5 eV $\div$ $+0.5$ eV) vicinity of the point where both bands touch each other, i.e., at $E \approx E_F \approx 0$ point. It is also supposed that the density of states within the graphene sheet bands is $\rho(E)$ $[(\text{eV} \times \text{at.})^{-1}] = 0.041|E|$, where E is in eV and the concentration of delocalized itinerant π-carriers in sheets at $T = 0$ is determined as $N[\text{at.}^{-1}] = \int \rho(E)\text{dE} \approx 0.02|E_F|^2$. Unlike aforementioned 5–7 nm nanoparticles where the number of carbon atoms per particle is $\sim 10^4$ and the number of mobile carriers is quite small, reaching 6 even at the extremely large $E_F = 0.17$ eV, for the astralen particle the corresponding numbers are 5×10^6 and 500–5000 (expected value based on the estimated values $|E_F| \sim 20$–30 meV) that allow disregarding the discrete origin of electric charge. The experimental data fitting by Eq. (1) (Fig. 6(c)) provides us with the following parameters $|E_F| \approx 13$ meV and $\Delta T = 338$ K. These values evidence on quite high quality of graphene layers in astralen particles though in some MWCNT the graphene sheet quality seems to be even higher: $\Delta T = 190$ K[16] and $\Delta T = 110$ K.[21] The absolute value of in-plane orbital susceptibility of astralen is $|\chi_{orb}| \approx 21 \times 10^{-6}$ emu/g at $T = 260$ K. This value is close to the corresponding values found for graphite particles with sizes above 10 nm[14] and bulk graphite. At the same time for MWCNT the $|\chi_{orb}|$ values at $T = 260$ K are found to be about 15% higher than in astralen.[18]

Let us estimate the stability of the parameters $|E_F|$ and ΔT found for astralen depending on the model in use: (1) $\chi_P = 0$, $E_F = f(T)$; (2) $\chi_P = \text{const}$, $E_F = f(T)$; (3) $\chi_P = 0$, $E_F = \text{const}$; (4) $\chi_P = \text{const}$, $E_F = \text{const}$. The first model has been analyzed above. Model 2 provides $|E_F| \approx 18.5$ meV, $\Delta T = 307$ K, $\chi_p = 0.43 \times 10^{-6}$ emu/g; model 3-$|E_F| \approx 21$ meV and $\Delta T = 306$ K; model 4-$|E_F| \approx 23.5$ meV, $\Delta T = 275$ K, $\chi_p = 0.33 \times 10^{-6}$ emu/g. One may conclude that the Pauli susceptibility in astralen can not exceed $\chi_p = 0.43 \times 10^{-6}$ emu/g i.e., of the same order of magnitude as for 5–7 nm multishell polyhedral nanographites, and the confidence interval for the ΔT-value lies within the $275 \div 338$ K interval. The most sensitivity and dispersion demonstrates the $|E_F|$–parameter: from 13 to 23.5 meV. The upper limit of 23.5 meV ($\sim$270 K) well corresponds to typical $|E_F|$-values in MWCNT where sources of extrinsic carriers are both acceptor type point-like defects in graphene layers and linear edge defects.[22] At the same time the estimation of $(k_B\Delta T)/E_F$ ratio for all models under consideration gives surprisingly conservative values $1.0 \div 2.2$ whereas for other nanocarbon materials (nanotubes, nanographites) with linear edge defects this value is about 0.5.

Our recent HRTEM, XRD and Raman spectroscopy studies[10] revealed and confirmed a polyhedral multi-shell fullerene-like structure of astralen particles that consist of large flat sp^2 graphene faces connected by defective corner regions with presumably pentagon-like structure. The spacing of lattice fringes of 0.340 nm is larger than the (002) inter-plane distance in graphite (~0.335 nm) but smaller than the corresponding value in polyhedral carbon onions from HT annealed nanodiamonds (0.345 nm[8] and 0.353 nm[6]). In addition to this structural data, multi-frequency EPR and magnetic susceptibility measurements provide unique information on the electron structure and magnetic properties of this large closed π-electron network. It is obvious that astralen takes its special place among the whole family of nanographite particles with crystallite sizes from 3 to 50 nm. Astralen combines two unique and, prima facie, hardly matching properties. On the one hand astralen, like nanographites with the crystallite size ~3.5 nm, has the highest available concentration of the edge spin states (~6.7×10^{18} spin/g). On the other hand, as it should be for well developed defect-free graphite particles with crystallite sizes above 10 nm, astralen shows practically the highest value of in-plane orbital susceptibility that corresponds to the value of bulk graphite $\chi_{orb}(300\ K) = -22 \times 10^{-6}$ emu/g. It may be supposed that π-electrons in the astralen graphene layers should effectively propagate exchange interaction between edge spins that corresponds well with the low-field g-shifts of the EPR lines originated from the edge localized defects.

In summary we report unusual electronic and magnetic properties of the astralen nanoparticles and discuss them in terms of the hypothesis that each astralen nanoparticle constitutes a closed network of delocalized π-electrons. This feature, in turn, is attributed to the multi-shell polyhedral structure of astralen and in particular to the fact that the polyhedra consist of large (~15 nm) defect-free sp^2 flat faces while a certain number of defects condenses at the polyhedral edges.

Acknowledgments: This work was supported, in part, by the Israeli Ministry of Immigrant Absorption. The authors acknowledge Professor S. Waplak, Dr. W. Bednarski and Dr.-hab. L. Piekara-Sady (Institute of Molecular Physics, Polish Academy of Sciences, Poznan) for providing multi-frequency EPR facilities.

References and Notes

1. H. W. Kroto, J. R. Heath, S. C. O'Brien, R. F. Curl, and R. E. Smalley, *Nature* 318, 162 (**1985**).
2. D. Ugarte, *Nature* 359, 707 (**1992**).
3. H. Terrones and M. Terrones, *J. Phys. Chem. Solids* 58, 1789 (**1997**).
4. S. Tomita, T. Sakurai, H. Ohta, M. Fujii, and S. Hayashi, *J. Chem. Phys.* 114, 7477 (**2001**).
5. P. V. Pikhitsa, Y. J. Kim, M. W. Kim, S. Yang, T. W. Noh, and M. Choi, *Phys. Rev. B* 71, 073402-1 (**2005**).
6. O. E. Andersson, B. L. V. Prasad, H. Sato, T. Enoki, Y. Hishiyama, Y.Kaburagi, M. Yoshikawa, and S. Bandow, *Phys. Rev. B* 58, 16387 (**1998**).
7. B. L. V. Prasad, H. Sato, T. Enoki, Y. Hishiyama, Y. Kaburagi, M. Yoshikawa, A. M. Rao, P. C. Eklund, and M. Endo, *Phys. Rev. B* 62, 11209 (**2000**).
8. V. Yu. Osipov, T. Enoki, K. Takai, K. Takahara, M. Endo, T. Hayashi, Y. Hishiyama, Y. Kaburagi, and A. Ya. Vul', *Carbon* 44, 1225 (**2006**).
9. A. N. Ponomarev and V. A. Nikitin, Layered fulleroid-type polyhedral carbon nanostructures, Patent RU 2196731, from 2000.09.21, filed on 2003.01.20.
10. A. I. Shames, E. A. Katz, A. M. Panich, D. Mogilyansky, E. Mogilko, J. Grinblat, V. P. Belousov, I. M. Belousova, and A. N. Ponomarev, *Diamond Relat. Mater.* 18, 505 (**2009**).
11. A. I. Shames, A. M. Panich, V. Yu. Osipov, A. E. Aleksenskiy, A. Ya. Vul', T. Enoki, and K. Takai, *J. Appl. Phys.* 107, 014318 (**2010**).
12. A. M. Panich, H.-M. Vieth, A. I. Shames, N. Froumin, E. Ôsawa, and A. Yao, *J. Phys. Chem. C* 114, 774 (**2010**).
13. D. Mustafi, E. V. Galtseva, J. Krzystek, L.-C. Brunel, and M. W. Makinen, *J. Phys. Chem. A* 103, 11279 (**1999**).
14. M. Kempiński, W. Kempiński, J. Kaszyński, and M. Śliwińska-Bartkowiak, *Appl. Phys. Lett.* 88, 143103 (**2006**).
15. S. Łoś, L. Duclaux, W. Kempiński, and M. Połomska, *Micropor. Mesopor. Mater.* 130, 21(**2010**).
16. H. T. Pinnick, *Phys. Rev.* 94, 319 (**1954**).
17. J. Winter, Magnetic Resonance in Metals, Clarendon Press, Oxford (**1971**), Chap. 10.
18. V. Likodimos, S. Glenis, N. Guskos, and C. L. Lin, *Phys. Rev. B* 68, 045417 (**2003**).
19. A. S. Kotosonov, *JETP Lett.* 43, 37 (**1986**); *JETP Lett.* 66, 1068 (**1987**).
20. A. I. Veinger, A. G. Zabrodskii, and T. V. Tisnek, *Semiconductors* 34, 746 (**2000**).
21. A. S. Kotosonov and V. V. Atrazhev, *JETP Lett.* 72, 53 (**2000**).
22. A. S. Kotosonov, *JETP Lett.* 70, 476 (**1999**).

Received: 24 June 2010. Accepted: 20 July 2010.